International Geology Review, Vol. 50, 2008, p. 1–25. DOI: 10.2747/0020-6814.50.3.XX

The Nascent Coso Metamorphic Core Complex, East-Central California: Brittle Upper Plate Structure Revealed by Reflection Seismic Data

JEFFREY R. UNRUH,
William Lettis & Associates, Inc., 1777 Botelho, Suite 262, Walnut Creek, California 94596

FRANCIS C. MONASTERO,
Geothermal Program Office, Naval Air Weapons Station, China Lake, California 93555

SATISH K. PULLAMMANAPPALLIL
Optim Inc., 1664 N. Virginia Street, Reno, Nevada 89557-0001

Abstract

The relationships between upper crustal faults, the brittle-ductile transition zone, and underlying magmatic features imaged by multifold seismic reflection data are consistent with the hypothesis that the Coso geothermal field, which lies within an extensional step-over between dextral faults, is a young, actively developing metamorphic core complex. The reflection images were processed using a non-linear simulated annealing approach to invert P-wave first arrivals in the seismic data for 2-D velocity structure. Velocity tomograms obtained from the inversions were employed in a pre-stack Kirchhoff migration to produce depth-migrated images of subsurface structure. The seismic images reveal coherent reflectivity in the upper 5 km of the Mesozoic intrusive bedrock of the Coso Range. The Coso Wash fault and other late Pleistocene and Holocene normal faults in, and adjacent to, the geothermal field are expressed on the reflection images by lateral truncations of coherent reflectors, and locally as discontinuous planar reflectors down-dip of the surface fault traces. The faults appear to terminate downward against a faint, subhorizontal, discontinuous reflective horizon ("A") at about 4 km depth that lies at or near the base of seismicity beneath the geothermal field. This horizon is interpreted to be the brittle-ductile transition zone. The seismic images also reveal a prominent high-amplitude reflector at 6 km depth directly beneath the geothermal field, and a deeper reflective horizon at a depth of about 8 to 9 km. These deeper reflectors are associated with a zone of low P- and S-wave velocities in the 6–12 km depth range beneath the geothermal field, and are probably related to the presence of magma or other pressurized fluids. The combination of magmatic heat and active normal faulting in the regional transtensional setting establishes the conditions for hydrothermal convection in the Coso geothermal field.

Introduction

THE UPPER PLATE in all exhumed and well-studied metamorphic core complexes shows extensive brittle faulting and fracturing (Lister and Davis, 1989). Commonly there are multiple generations of high- and low-angle normal faults that cross-cut each other in a complicated network that accommodates brittle decomposition (Gans et al., 1985). With depth, the brittle faults sole into or terminate against a zone of mylonitized rocks that appear to be the result of deformation in mid-crustal ductile shear zones (Coney, 1979; Lister and Davis, 1989).

The basic structural model for a metamorphic core complex is shown in Figure 1, which is a cross-sectional representation parallel to the extension direction. It consists of a breakaway fault at the locus of maximum extension with numerous high-angle normal faults that accommodate that extension (Fig. 1). These faults become listric with depth and/or are rotated into a near horizontal orientation above the footwall (Spencer, 1984; Buck, 1988). The boundary that separates brittle behavior in the upper plate from ductile flow in the lower plate, referred to as the main detachment zone, commonly is bowed upward into an antiformal structure directly adjacent to the breakaway fault zone. This zone is at its shallowest near the breakaway fault, deepens with increasing distance from the breakaway, and presumably becomes more brittle (Gans et al., 1985)

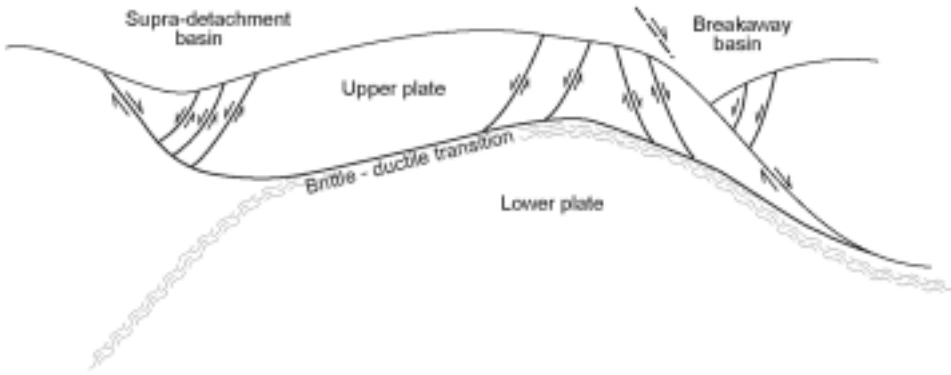

FIG. 1. Generalized model for a metamorphic core complex (after Gans et al., 1985).

because it is farther from the locus of uplift of the lower plate that is advecting heat to the near-surface. The distal termination of this detachment zone is characterized by one or more fault-bounded sedimentary basins that commonly have associated antithetic faults (Fillmore et al., 1994; Ingersoll et al., 1996; Fillmore and Walker, 1996; Gans et al., 1985). These supra-detachment basins principally receive sediments from the center of the uplifting core complex and commonly have admixed tuffs and lava flows from contemporaneous volcanism. Although the specific structural elements of any given core complex may differ from this basic model, all core complexes show a majority of these features.

Exhumed core complexes are a result of large extensional strains. Workers have inferred structure of core complexes early in their deformation history at low cumulative strains from palinspastic reconstruction of exhumed examples (e.g., Serpa and Pavlis, 1996), but natural examples of nascent, actively developing core complexes are sparsely documented. Monastero et al. (2005) proposed that the Coso geothermal field in eastern California is such an example. If this interpretation is correct, then active brittle faulting in the upper crust of the central Coso Range should be kinematically linked to ductile flow in the middle crust across a shallow brittle-ductile transition zone.

This paper presents new seismic images, neotectonic fault mapping, and seismicity of the Coso geothermal field (Fig. 2) to explore these structural and kinematic relationships. A total of 47 line-km of 2-D reflection data were acquired in the central Coso Range using a fairly standard acquisition approach. The data were processed using a new combination of detailed velocity modeling and Kirchhoff pre-stack migration techniques to obtain depth-migrated images of the subsurface structure (Pullammanappallil et al., 2001). A specific goal of this study was to image brittle faults and fractures in the upper 3 to 4 km of the crust that may control permeability and localize production in the geothermal field. Ancillary goals of this work included imaging the brittle-ductile transition, investigating for evidence of magmatic features in the middle crust, and assessing the relationship of these to the upper crustal faults.

The reflection data are used with seismicity and recent neotectonic mapping, done by the authors, of fault structures in the Coso field to define further the structure and transtensional setting of the nascent Coso metamorphic core complex described by Monastero et al. (2005). Evidence of brittle faults that cut Pleistocene and Holocene alluvial and pyroclastic deposits are abundant in the eastern part of the study area. Many of these faults spatially are associated with microseismicity, and appear to be transmissive structures in the geothermal field (Julian et al., 2007). The total data set permits a more comprehensive view of the structure of the Coso field and how that structure relates to regional tectonics. It also better enlightens us with regard to how various parts of exhumed core complexes functioned during the early stages of their formation.

Tectonic and Structural Setting of the Coso Range

The Coso Range is located in the tectonically active region within the transitional boundary

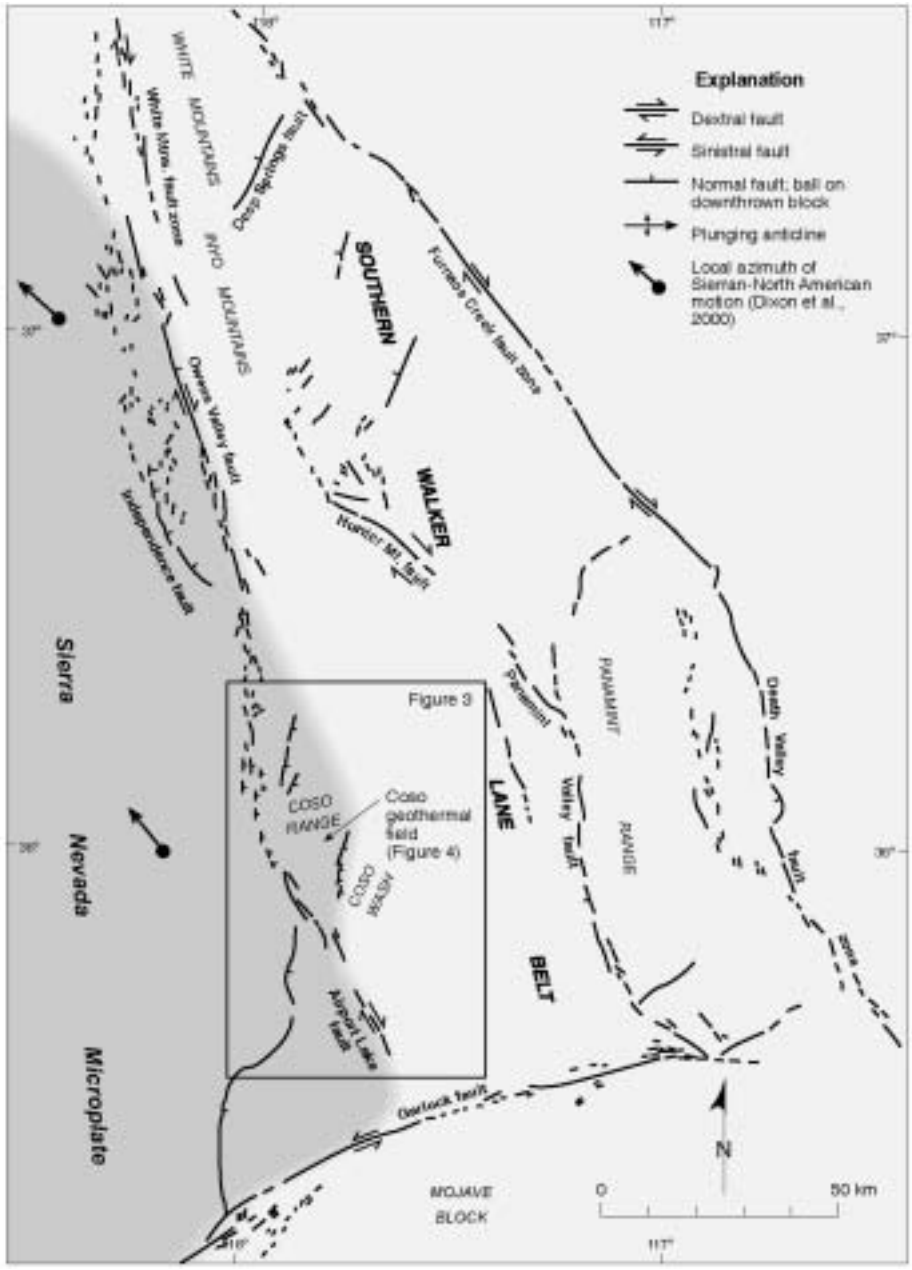

FIG. 2. Regional location map of the Coso Range and the southern Walker Lane belt. The extent of the rigid Sierra Nevada microplate is indicated by dark shading. Note right-releasing jog along the eastern margin of the Sierran microplate at the latitude of the Coso Range. Active faults in the southern Walker Lane belt from Jennings (1994).

between the Sierra Nevada–Great Valley (Sierran) microplate to the west and the Basin and Range to the east (Fig. 2). The former is moving northwest at a rate of 12–14 mm/yr relative to North America (Argus and Gordon, 1991, 2001; Dixon et al., 2000), resulting in dextral shearing and transtension along

the entire eastern Sierran front (Unruh et al., 2003). Deformation in the wake of Sierran motion is accommodated by distributed strike-slip and normal faulting in a 100 km wide zone variously known as the southwestern Basin and Range (Wernicke, 1992), the eastern California shear zone (Dokka and Travis, 1990), and the southern Walker Lane belt (Dixon et al., 1995, 2000; Unruh et al., 2003). Based on the Sierran block moving at N44°W (Dixon et al., 2000) and using the average orientation of the eastern front of the Sierra Nevada (N17W), Dewey et al. (2008, this volume) have calculated the direction of instantaneous maximum extension as N75.5W and the direction of maximum compression as N14.5E. These values are consistent with principal strain trajectories derived from inversion of earthquake focal mechanisms done by Unruh et al. (2002) for the Coso Range.

The Coso Range is situated in a right-releasing stepover between the Airport Lake and Owens Valley faults, which are two elements of the major dextral strike-slip system along the southeastern margin of the Sierran microplate (Fig. 2). The stepover between the faults drives oblique extension and the formation of the nascent Coso metamorphic core complex in the central Coso Range (Monastero et al., 2005). South of the Coso Range, dextral motion on the Airport Lake fault is distributed over a 5 to 15 km wide zone in eastern and northeastern Indian Wells Valley that is dominated by dextral strike-slip and normal-oblique (down-to-the-west) slip on NNW- to NNE-striking faults (Fig. 2). The distributed deformation is accommodated by three major branches or zones of faulting:

1. The eastern branch in northeastern Indian Wells Valley is characterized by north- to NNE-striking normal faults that extend into the area known as Wild Horse Mesa (Fig. 2), where they form a dramatic series of left-stepping structures with primarily west-facing scarps, ramps, and flats in Pliocene lava flows (Duffield and Bacon, 1981).

2. The central branch is a zone of N-S–trending, west-stepping faults in the Indian Wells Valley that occur south of, and extend into, the White Hills. These structures appear to transfer some of the dextral motion from the Airport Lake fault to the Coso Wash fault (Fig. 2). This left step in the strike-slip system is likely responsible for formation of the WNW-striking, ESE-plunging White Hills anticline as a fault-induced fold (Monastero et al., 2002).

3. The western branch of this zone of distributed faulting is marked by the NW-striking Little Lake fault zone. Roquemore (1981) documented approximately 250 meters of dextral strike-slip offset on a 440,000-year-old basalt flow cut by the Little Lake fault, implying a long-term average Quaternary slip rate of 0.58 mm/yr. This fault curves around the southwest margin of the Coso Range into Rose Valley, where the strike becomes more northerly and the fault disappears beneath alluvial fans extending eastward from the Sierra Nevada. A large earthquake swarm in 1982 in the northwest Indian Wells Valley featured a magnitude-5.2 event, whose focal mechanism and aftershock pattern indicated displacement on a NW-striking fault. This earthquake was attributed to the Little Lake fault by Roquemore and Zellmer (1983).

Strain Transfer Through the Coso Range

Based on the geomorphic expression of the faults in late Quaternary deposits, the bulk of Holocene deformation in the Coso Range is associated with the central branch of the Airport Lake fault zone. The most significant structure in this branch is the Coso Wash fault, which consists of a series of NNE-striking, normal faults that dip both to the SSE and the WNW. This fault zone extends from the White Hills anticline northward to Haiwee Spring in northern Coso Wash (Fig. 3), and is interpreted to be the principal locus for transferring active dextral shear through the Coso Range.

The Coso Wash fault zone can be traced about 9 km north of Airport Lake playa as a series of SE-dipping structures that have clear expression as scarps in Holocene alluvial fan deposits. The fault along this reach consists of a series of alternating short NNE- and NW-striking reaches (Fig. 3). At the southern margin of the geothermal field, in the vicinity of the active fumaroles shown in Figure 4, the orientation of the faults determined from field mapping abruptly changes from SSE-dipping to a predominance of a WNW-dipping structures (Figs. 3 and 4). The active traces step northwest from the Coso Wash fault into the bedrock of the Coso Range, and dip toward the main producing zones of the geothermal field. The WNW-dipping fault segments are geomorphically well expressed by northwest-facing scarps in bedrock and alluvium, and the faults locally pond alluvium in their downdropped hanging wall blocks upstream of the scarps. Ephemeral stream valleys that cut across the faults have pronounced nickpoints and are significantly more incised on their up-thrown sides. At least one of the

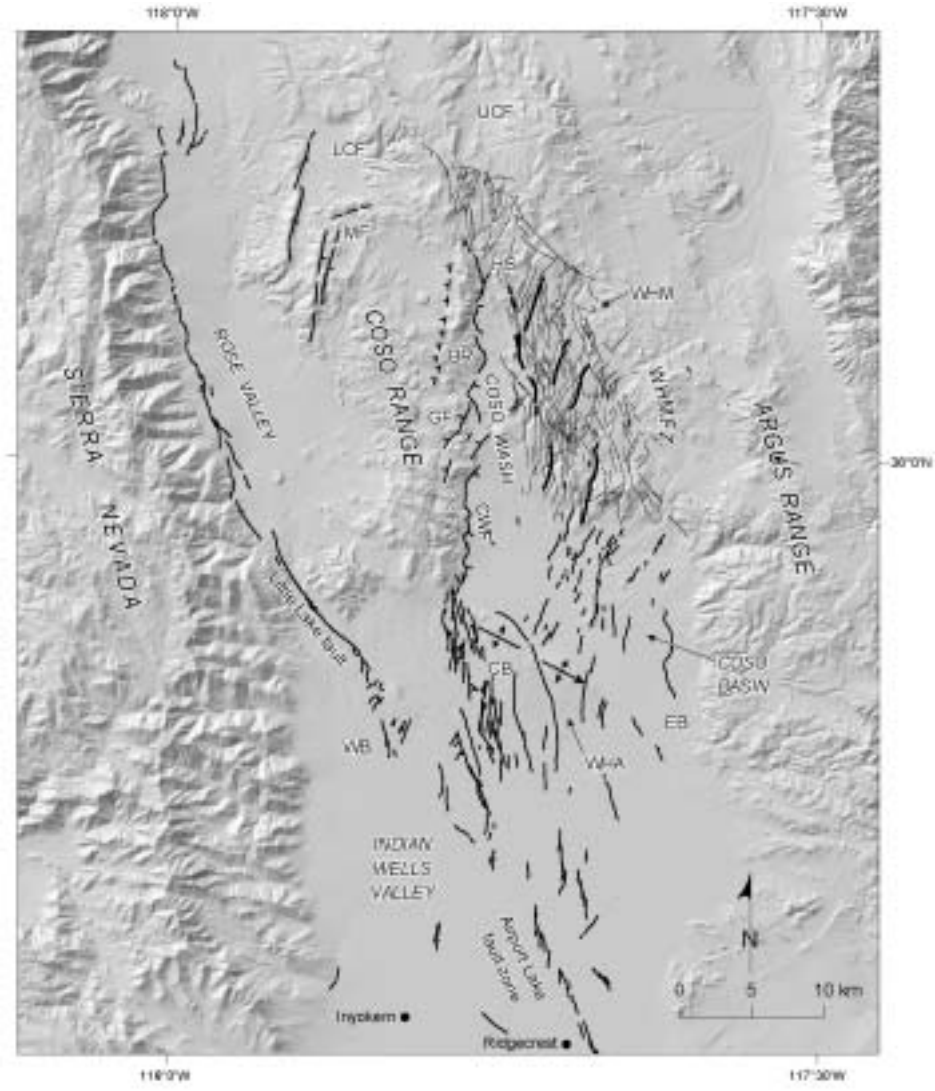

FIG. 3. Active splays of the northward branching Airport Lake fault zone in northern Indian Wells Valley, Rose Valley, the Coso Range, and Wild Horse Mesa. Holocene-active faults modified from Whitmarsh (1997) and mapping by the authors. Fault splays in Wild Horse Mesa with especially prominent geomorphic expression (and thus possibly accommodating greater slip) highlighted in bold. Abbreviations: WB = Western Branch; CB = Central Branch; EB = Eastern Branch; WHM = Wild Horse Mesa; WHMFZ = Wild Horse Mesa fault zone; CWF = Coso Wash fault; GF = geothermal field; BR = "basement ridge"; HS = Haiwee spring; UCF = Upper Cactus Flat; LCF = Lower Cactus Flat; MC = McCloud Flat.

NNE-striking, WNW-dipping normal faults is associated with active fumaroles (Fig. 4).

The east-dipping Coso Wash fault and the WNW-dipping normal faults collectively bound a prominent NNE-trending basement ridge that separates Coso Wash from the main production area of the Coso geothermal field (Walker and Whitmarsh, 1998). As a fault-bounded feature, the basement ridge is about 23 km long (Fig. 3), locally exhibits up to 550 meters of relief, and is best expressed between the geothermal field and Haiwee Spring. The basement ridge in the central Coso Range is

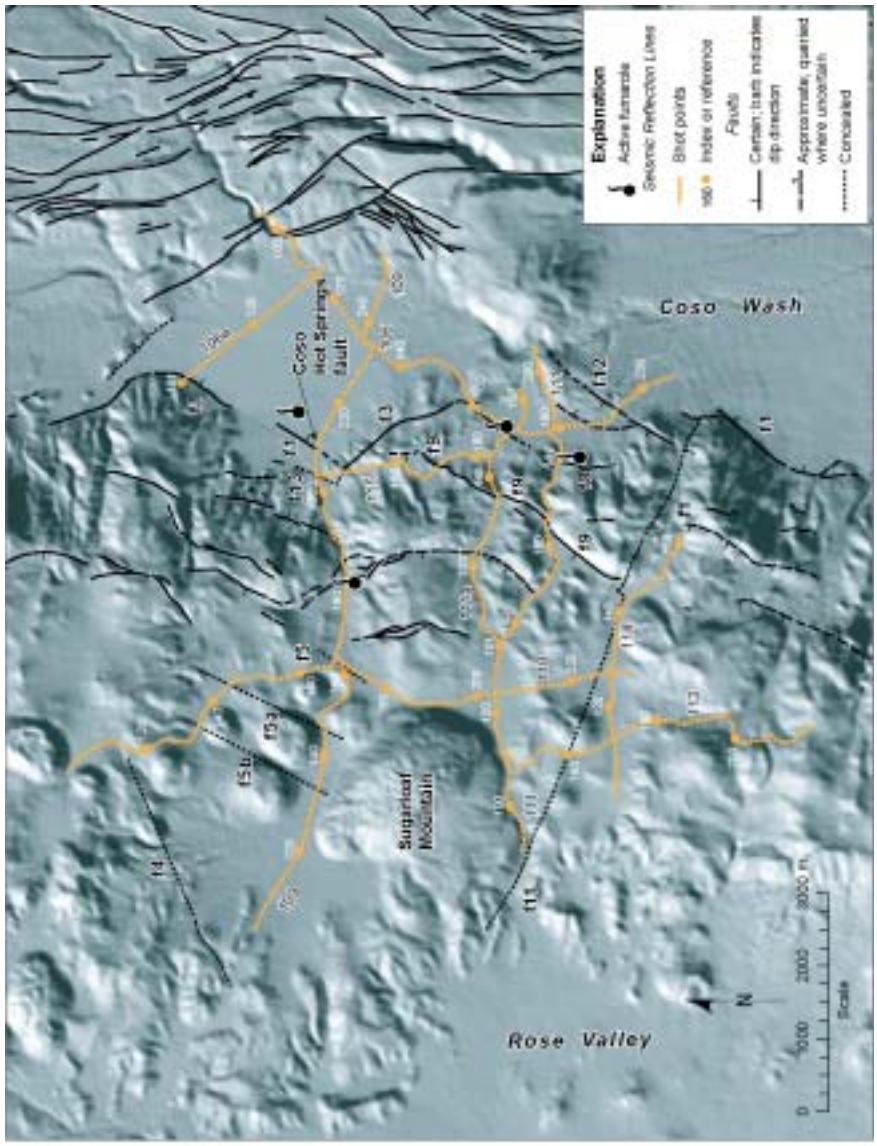

FIG. 4. Late Quaternary faults and locations of seismic reflection lines in the Coso geothermal field (see Fig. 2 for location).

essentially a horst block and may be analogous to the "central ridge" that Dooley et al. (2004) observed in scaled analog models of transtensional releasing stepovers that include a ductile substratum beneath a simulated brittle upper crust (quartz sand).

Some of the WNW-dipping segments of the Coso Wash fault terminate against a NW-trending bedrock feature mapped as a "tectonic breccia zone" (TBZ) by Whitmarsh (1997), and labeled as f_3 in Figure 4. The TBZ (f_3) is distinguishable as a prominent white tonal lineament on air photos, and is characterized by a zone of sheared and highly comminuted granite that exhibits local hydrothermal alteration. The scarp and associated alteration zone of the SE-dipping Coso Hot Springs (CHSF) segment of the Coso Wash fault (Fig. 4) can be traced to within 10 m or less of the TBZ. Based on the alteration of the TBZ and its structural relationship with the CHSF, we interpret this feature to be a displacement transfer structure that accommodates the change in vergence between the NW-dipping segments of the Coso Wash fault within and adjacent to the geothermal field, and the SE-dipping CHSF. Fluvial deposits that cross the southern part of the TBZ are also locally faulted with NE-facing scarps indicating late Holocene north-down motion resulting from slip on the CHSF.

North of Coso Hot Springs, the Coso Wash fault (f_1 on Fig. 4) dips consistently ESE and can be traced as a series of east-facing scarps in Holocene alluvium northward to the area around Haiwee Springs, where it loses its surface expression (Fig. 3). Farther north from Haiwee Springs, Coso Wash terminates as a Quaternary basin and narrows to a steep canyon cut in Cretaceous bedrock and Pliocene basalts of Wild House Mesa. Analysis of stereo aerial photography of this segment of the fault indicates east-facing bedrock scarps, and possibly fault-related east-facing bedrock slopes. These features probably represent Quaternary faulting, as recognized earlier by Walker and Whitmarsh (1998). The step-faulted terrain associated with the eastern branch of the Airport lake fault and the Coso Wash fault appear to merge at this location to form a rhombic array of faults at the southern terminus of Upper Centennial Flat (Fig. 3), near and east of the northern termination of the basement ridge.

In the north-central part of the Coso Range, the locus of active deformation steps left westward as a series of NNE-striking, left-stepping normal faults that bound the western margins of Quaternary basins such as McCloud Flat and Lower Cactus Flat (Fig. 3). The geomorphic expression and relative activity of these structures appear to increase northward as slip dies out on the Coso Wash fault and basement ridge to the east. The large-scale, left-stepping pattern of normal faults in the Coso Range is consistent with accommodation of NW-directed dextral transtension.

Reflection Seismic Data

Acquisition of useful reflection seismic data in the Coso geothermal area is contingent on successfully dealing with several significant factors. The bedrock of the central Coso Range west of Coso Wash consists of Mesozoic intrusive and metamorphic rocks that are lithologically and temporally equivalent to those of the Sierra Nevada batholith (Duffield et al., 1980). The crystalline bedrock beneath the geothermal field is overlain by a relatively thin veneer (0 to 300 meters) of Pleistocene extrusive and pyroclastic volcanic rocks (Duffield and Bacon, 1981; Whitmarsh, 1997), including a rhyolite dome field (Duffield et al., 1980). This setting creates a challenge for seismic data acquisition and processing design to deal with low signal to noise ratio (Juhlin and Palm, 1999), intense wave scattering (Eaton et al., 2003), small reflection coefficients between rock bodies (Salisbury et al., 2003), and shallow low-density zones that create major static correction problems. Areas of intense hydrothermal alteration and basins filled with low-density pyroclastic material also act to absorb incident energy, thus attenuating the signal.

Our selection of acquisition parameters, line geometry, and data processing methods specifically addressed these issues. A total of 47 km (29 mi) of seismic reflection data were acquired using standard Vibroseis technology over nine lines covering the main production area of the Coso geothermal field (see Fig. 4). Shot spacing was 134 m (440 ft) and receiver groups were spaced over 67 m (220 ft). Ten linear sweeps per station were used, each 10 seconds in duration with a 5 second listen time. The sweep frequency range was 5 hz to 50 hz, and data were acquired at a 2 ms sample rate. Table 1 provides a summary of some relevant parameters for the data on a line-by-line basis. The primary objective of selecting these array parameters was to acquire the longest possible offset data for first-arrival analysis in the processing phase, and the secondary

TABLE 1. Data Acquisition Parameters

Line no.	No. of shots	No. of recs	Max. off., mi	Length, mi	Length, km
106	62	114	3.5	3.75	6.0
106a	36	39	1.53	1.6	2.6
109	121	155	5.1	5.9	9.5
110	94	132	4.65	4.85	7.8
111	85	116	4.0	4.3	6.9
111a	40	62	1.50	2.2	3.5
113	48	76	2.60	2.7	4.3
114	34	62	1.74	2.3	3.7
115	29	47	1.65	1.65	2.7
Total				29.25	47.3

objective was to achieve resolution sufficient to delineate major structures.

Reflection seismic data were processed using the non-linear simulated annealing optimization approach described fully in Pullammanappallil and Louie (1993, 1994). P-wave first arrivals in the seismic data were inverted to obtain the 2-D velocity structure along each seismic line. SeisOpt @2D, a proprietary inversion algorithm that employs a non-linear simulated annealing approach, was used to randomly perturb an arbitrary starting model until the synthetic seismic wave travel times computed through it match the travel times picked from the raw data. In addition to accepting perturbed models that have lower travel-time error, the algorithm conditionally accepts models with larger error. As annealing proceeds, conditional acceptance becomes less and less likely. Unlike linearized iterative inversions, simulated annealing optimization finds the global minimum while avoiding local error minima. It is completely insensitive to the starting velocity model, and requires no *a priori* assumptions about subsurface geologic or velocity structure. These characteristics make the method well suited for application to the Coso data set.

Two-dimensional velocity models (i.e., tomograms) were derived for all nine seismic lines (e.g., Fig. 5). Line length and array geometry were sufficient for first-arriving rays to sample the velocity structure to an average depth of about 600 m, and to a maximum depth of about 1200 m for the longest lines. Velocities in the upper 150 m to 300 m depth are in the range of 0.9 to 3 km/s (~915 to 3,050 m/s: Fig. 5). West of Coso Hot Springs fault, velocities that characterize intrusive and metamorphic rocks below a depth of 300 m typically are 4.1 km/s or greater (i.e., ~3,650+ m/s; Fig. 5). Velocities in the same depth range east of the Coso Hot Springs fault are lower, probably due to the presence of a thicker sequence of poorly consolidated basin fill in Coso Wash (Fig. 5).

The velocity models were extended in depth (Optim LLC, 2003) by performing a joint hypocentral-velocity inversion of microearthquake P-wave first arrivals using the method of Asad et al. (1999). This permitted extension of the velocity model to depths in excess of 7600 m.

Kirchhoff pre-stack, depth-migrated images were developed for each seismic line by using the velocity tomograms as a basis for migrating the reflection data. Prestack depth migration involves little to no pre-processing of the seismic data, and each raypath through the input velocity model is individually imaged. This approach preserves information contained in the raw data and focuses coherent reflections within laterally complex velocity models. In contrast, conventional migrations involving use of stacking velocities assume lateral homogeneity of velocity models. This assumption tends to breakdown in areas of complex structure such as Coso. The Kirchhoff pre-stack migration as implemented for this study does not require definition of ray path. The ability to calculate travel times from Vidale's (1990) method for laterally heterogeneous structures avoids the limitations of straight ray approximations. The summation of the value of each

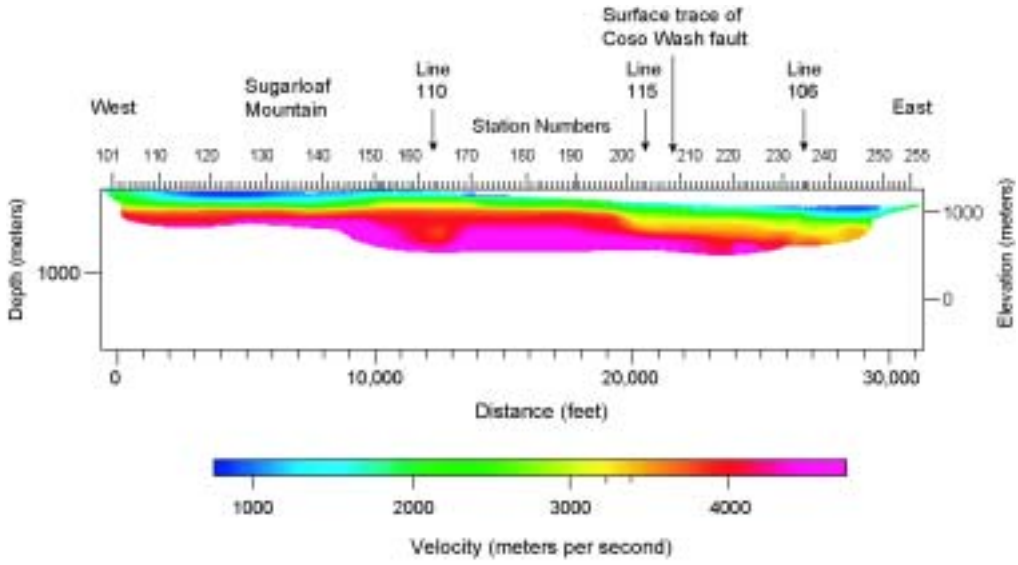

FIG. 5. Velocity tomogram for line 109 obtained from inversion of first arrivals in the seismic reflection data. Similar tomograms were derived for all seismic lines and used to perform a Kirchoff pre-stack depth migration.

seismogram (i.e., the amplitudes) at specified times will produce images of structures that cause lateral variations in impedence. The summation of arrival times may be made in any order, as the Kirchhoff summation method embraces the geometrical configuration of the source, receiver, and reflector as a function of time.

Results and Interpretation

Sources of reflectors

With the exception of the lines acquired in the sediment-filled Coso Wash (Fig. 3), the majority of the reflection data were collected from areas underlain by the plutonic and metamorphic basement that hosts the geothermal field. Among the many possible causes for reflectivity in the subsurface at Coso, three stand out as likely sources of impedance contrasts within the crystalline rocks that may produce the reflections in the data: (1) contacts between intrusive bodies of varying mineralogy; (2) hydrothermal alteration; and (3) fault zones filled with gouge.

In general, acoustic impedance (Z) for rocks, which is defined as the product of P-wave velocity (v_p) and density (p),

$$Z = v_p p \qquad (1)$$

increases with increasing mafic content (Christensen, 1996). The reflection coefficient (R) for a normal incidence P-wave is defined as

$$R = \frac{Z_2 - Z_1}{Z_2 + Z_1} = \frac{v_{p2}\rho_2 - v_{p1}\rho_1}{v_{p2}\rho_2 + v_{p1}\rho_1}. \qquad (2)$$

Salisbury et al. (1996) state that there need be only a 6% (R = .06) impedance contrast to obtain clear reflections from a planar surface. This translates to a density difference of 2.5×10^5 gm^{-1}, which is approximately the difference between a granite and a diorite. Whitmarsh (1997) and Walker and Whitmarsh (1998) mapped the full range of calc-alkaline plutonic rocks (from granite to gabbro) in the Coso Range and found that they are commonly intermingled in a so-called "mixed-complex" of mafic and felsic components. In spite of the fact that it is theoretically possible for such contacts to be subsurface reflectors, they must be more or less planar. Typical contacts between plutons are irregular in shape, resulting in scattering of acoustic waves (Eaton et al., 2003); based on lithologic data from drill holes in the geothermal field, Coso is no exception. It is difficult, therefore, to interpret what appear to be planar reflectors as intrusive contacts, which are more likely to be irregular. It is possible that some of the seismic reflectors represent tabular

dikes, but exposed dikes in the Coso geothermal field are only a 1–3 m in width, and thus below the level of resolution of these data.

Hydrothermal alteration can cause a sufficient change in rock density to produce an impedance contrast between altered zones and unaltered bedrock. Some of the bright, negative-amplitude, horizontal reflectors in the depth range of 300–500 m on line 109 (s.p. 175–220; Fig. 6) correlate with outcrops of intense argillic alteration found at Devil's Kitchen and Coso Hot Springs. Other areas in the Coso field where there is abundant hydrothermal alteration on the surface or in the subsurface, as determined from well data, do not exhibit similar types of reflections. We conclude, therefore, that hydrothermal alteration probably is not a consistent source of seismic reflectors in the data.

Faults and associated breccia zones also may be major sources of reflectors. In a setting dominated by plutonic rocks that have little in the way of horizontal continuity, fault zones are the major source of planar, or near planar, reflectors that extend over distances of several hundred meters. Mair and Green (1981), Kim et al. (1994), and Juhlin and Palm (1999) have all demonstrated the feasibility of imaging faults and fracture zones in crystalline basement rocks. Many of the reflectors that were observed in the Coso seismic data correlate with faults that crop out on the surface and/or are indicated in the subsurface data from wells. The approach that we took in interpreting the data, however, was not to look for the surface faults first and then determine if there were reflectors in the seismic sections. Instead, we first located reflectors in data, and then went to the geologic maps to see if there were correlations with mapped faults, and in many instances there were. We assume that most of the reflectors discussed in the following sections are fault-related, and we use abrupt lateral truncations of coherent reflectors to infer the down-dip continuation of surface faults. Wherever we believe that reflectors arise from features other than fault structures, we specifically state that in the text. Regardless of the specific origin of the impedance contrasts, we infer that the coherent reflectivity in the seismic data arises from real variations in rock properties.

As an example of our interpretive approach, we observed a west-dipping reflector in seismic line 109 (Fig. 6) that projects to the surface in the vicinity of s.p. 185, and which systematically cuts across subhorizontal to gently arcuate reflectors in the upper 2000 m between s.p. 153 and s.p. 185. We interpret this reflector as fault f_{13} (Fig. 6), and observe that its surface projection is coincident with a WNW-dipping fault along the western boundary of the bedrock ridge (Fig. 4); this structure also is associated with fumaroles, argillic alteration, and other surface manifestations of shallow hydrothermal activity. Similarly, we observed that an arcuate reflector or reflective horizon at a depth of about 1500 m below s.p. 150 on line 109 appears to be abruptly terminated or truncated to the west below s.p 143 (Fig. 6). Although the truncation of the subhorizontal reflector is not associated with a discrete west- or east-dipping reflector as in the previous example, we interpret the abrupt termination to be a consequence of faulting, and infer the presence of a west-dipping fault (i.e., fault f_{5a}; Fig. 6) along that and a series of other truncated and/or disrupted reflectors in the upper 1500 m depth range, approximately between s.p. 120 and s.p. 140. In contrast to fault f_{13}, fault f_{5a} has no obvious surface expression, but it is spatially associated with a series of three late Pleistocene rhyolite domes that are aligned along a WNW trend (Fig. 4).

Despite the large number of potential data problems in the Coso geologic setting, we found the upper 4 to 5 km of the crystalline crust beneath the geothermal field to provide good reflective structures. Some of the most prominent reflectors can be correlated on intersecting reflection lines, indicating that they arise from real impedence contrasts and are not processing artifacts. For example, there is a set of distinct reflectors with an apparent dip to the west at a depth of about 1.5 km between shotpoints 140 and 165 on line 109 (Fig. 6) that precisely match subhorizontal to gently south-dipping reflectors in the same depth range between shotpoints 160 and 175 on crossing line 110 (Fig. 7; see Fig. 4 for location). Although we cannot determine the lithologic source of the reflectors, the fact that they occur on two different seismic lines at high angles to each other indicate that the reflectors arise from real southwest-dipping features in the subsurface.

Brittle faults of the Coso geothermal area

Western boundary of Coso Wash. The fault within the seismic array with the most prominent geomorphic expression is the NNE-striking, ESE-dipping CHSF segment of the Coso Wash fault zone (Fig. 4), which is imaged on seismic lines 109, 106, and 106a (Figs. 6, 8, and 9, respectively). On line 109,

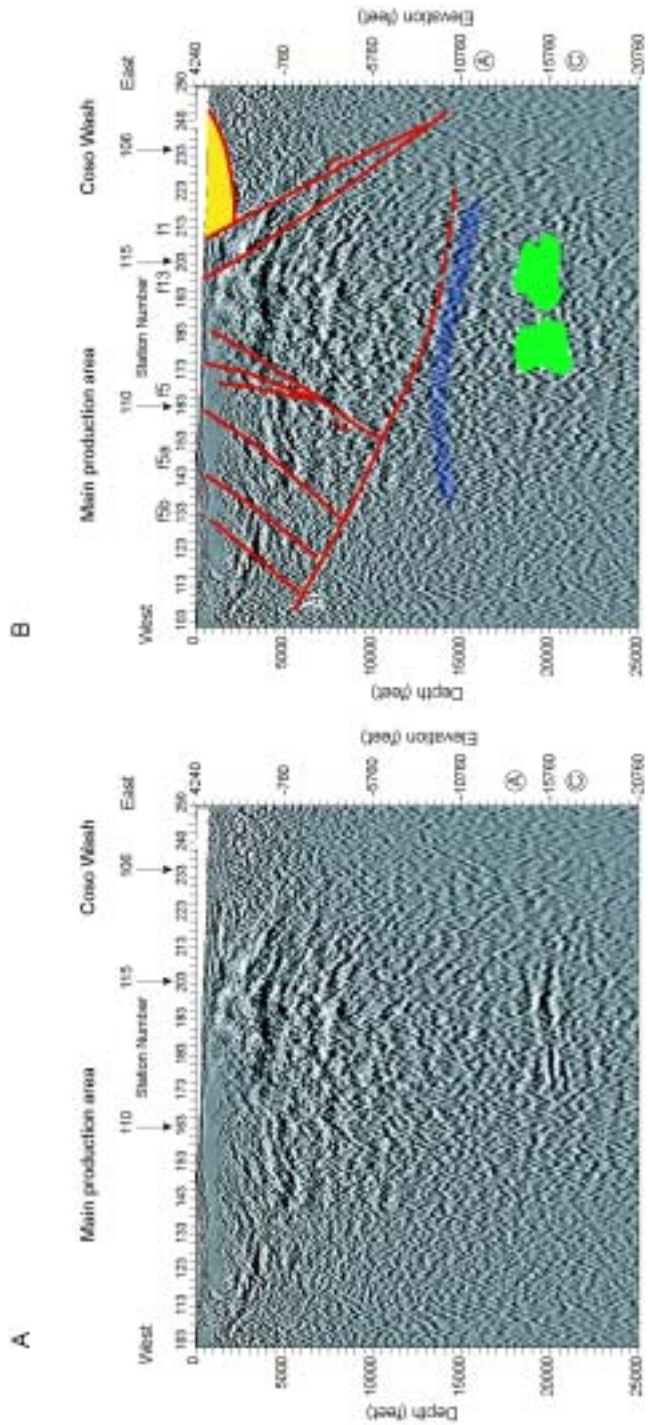

FIG. 6. Reflection line 109. A. Seismic data. B. Interpretation.

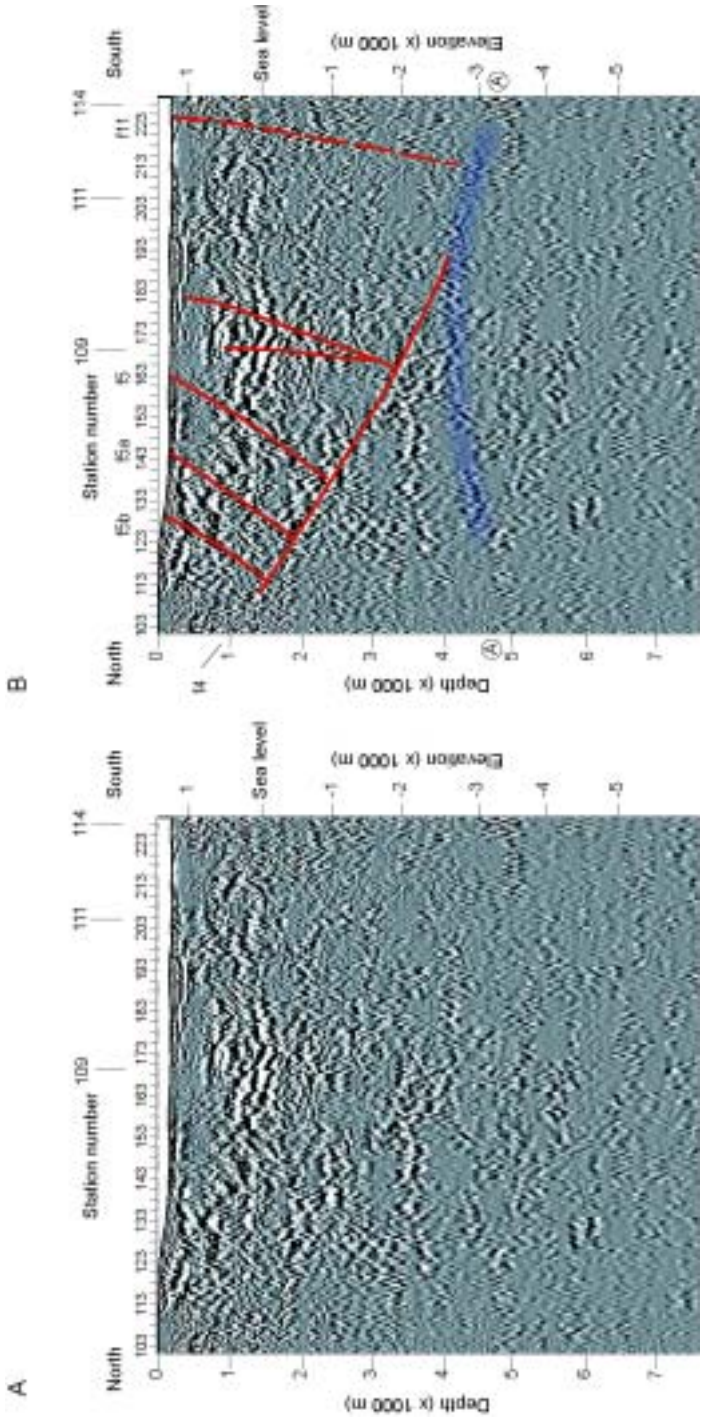

FIG. 7. Reflection line 110. A. Seismic data. B. Interpretation.

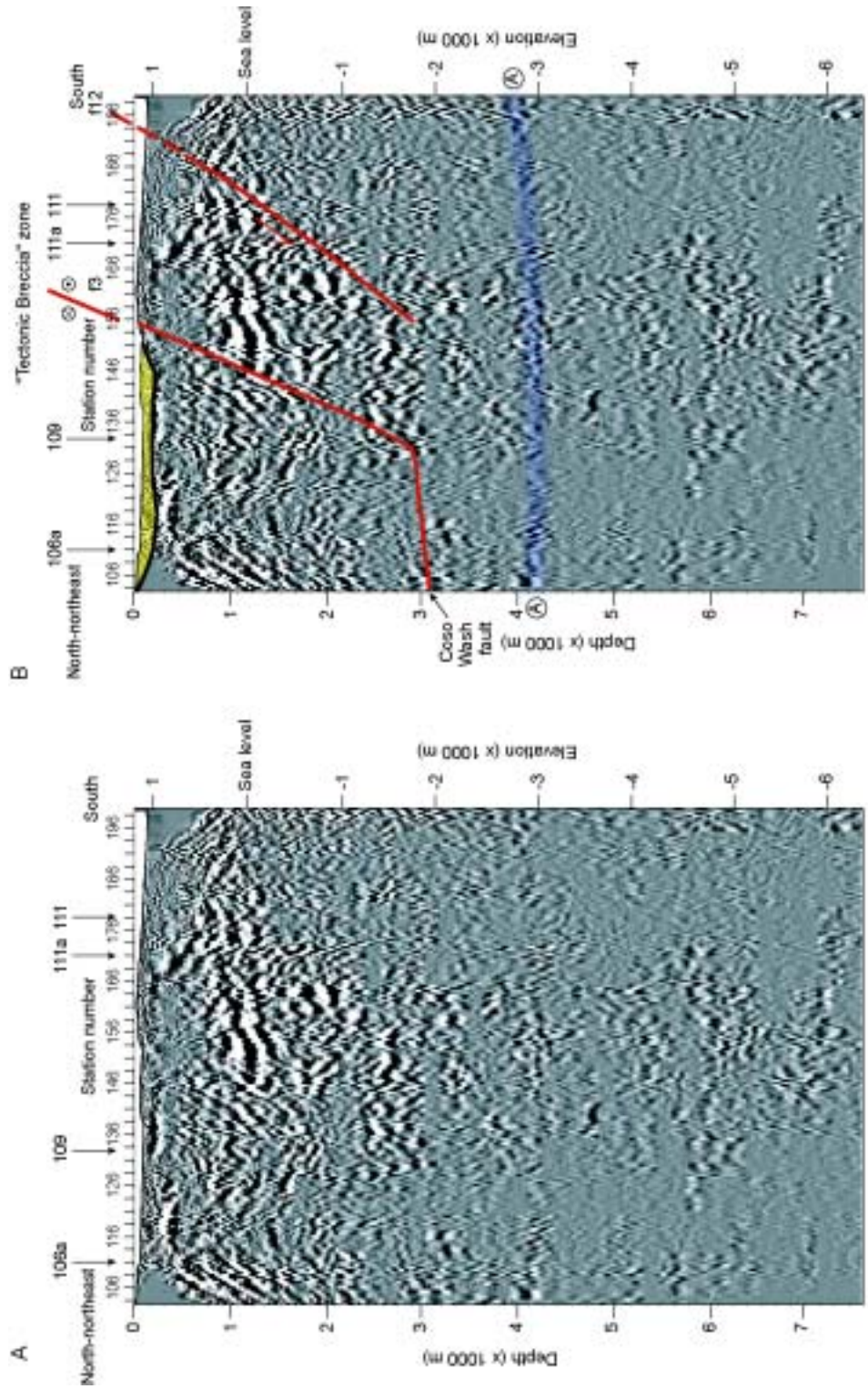

FIG. 8. Reflection line 106. A. Seismic data. B. Interpretation.

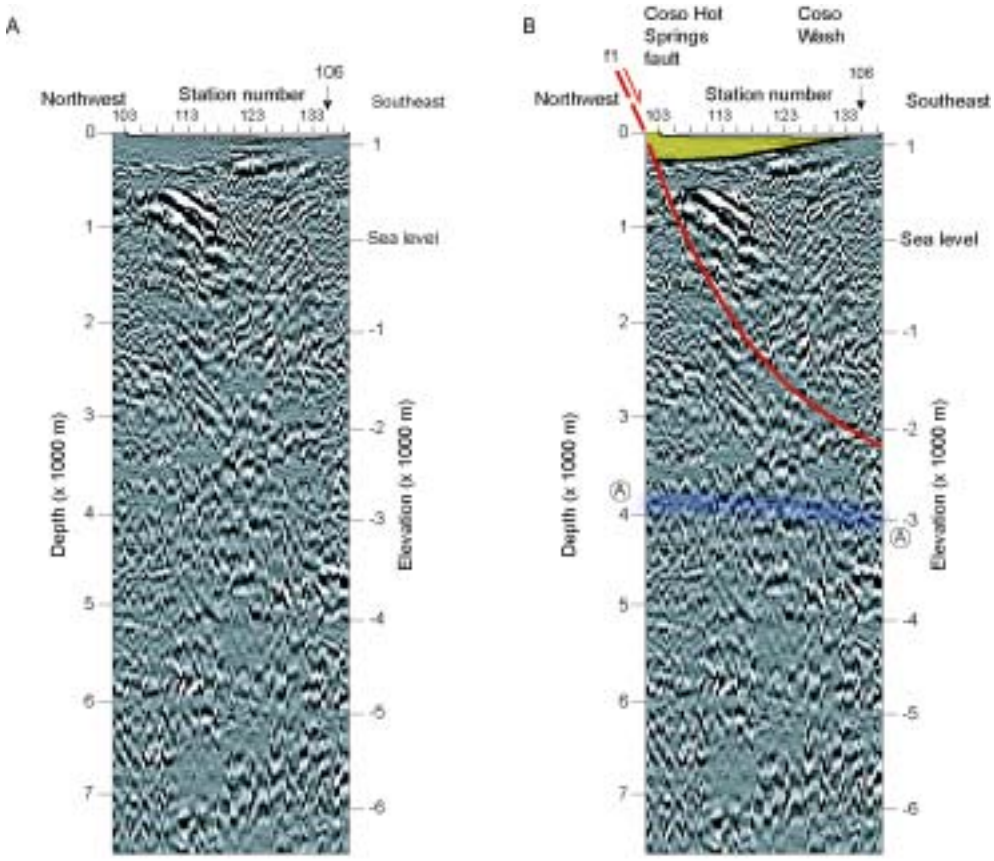

FIG. 9. Reflection line 106a. A. Seismic data. B. Interpretation.

the CHSF is imaged as a faint, east-dipping reflector that is associated with east-down displacement of shallow layered reflectors that we associate with alluvium in Coso Wash. The bedrock-alluvium contact beneath Coso Wash dips toward the northwest and terminates against the CHSF below s.p. 213; this intersection is downdip of a 3 m scarp in late Quaternary deposits exposed at about shotpoint 208 (Fig. 6). Based on the occurrence and concentration of hot springs, fumaroles, and mud pots along the fault trace, this structure clearly is a conduit for geothermal fluids to reach the surface. The CHSF has a similar appearance on reflection line 106a (Fig. 9), where the basement reflector beneath the alluvium of Coso Wash dips into, and terminates against, the east-dipping fault plane at a depth of about 530 m (1750 feet) beneath s.p.105. We infer down-dip continuation of the CHSF to be associated with the juxtaposition of west-dipping reflectors in the hanging wall. These reflectors, and east-dipping reflectors in the footwall, are probably interbedded Pliocene volcanic rocks and fluvial deposits of the Coso Formation, both of which are exposed at the foot of Wild Horse Mesa approximately 4 km to the east of the surface outcrop of the CHSF (Duffield and Bacon, 1981).

We infer that the CHSF is present in both lines 106 and 106a in the subsurface (Figs. 8 and 9, respectively), although the fault is not well imaged as a discrete reflector in these lines. As shown in Figure 4, the CHSF intersects the TBZ at depth of about 3000 m beneath s.p.130 on line 106 (Fig. 8). We interpret a steeply north-dipping alignment of truncated high-amplitude reflectors in the depth range of 1000 m to 2000 m on line 106 below the surface trace of the TBZ at s.p. 156 to be the down-dip continuation of this structure. It appears to form the southwestern structural boundary of the CHSF,

and as mentioned earlier, is likely a strain transfer structure linking north-south– to NNE-SSW–trending normal faults (Fig. 8).

Northwest-dipping segments of the Coso Wash fault south of the TBZ can be seen on seismic lines 111 and 111a (Figs. 10 and 11). These features have surface expression in scarps in Holocene sediments. In the subsurface they are distinguishable as lateral truncations of reflective features, and are locally associated with short, discontinuous, west-dipping reflectors. For example, fault f_9 on line 111 is associated with faint west-dipping reflectors that truncate or disrupt the continuity of reflectors at depths of about 1500 m and 3000 m (Fig. 10). These discontinuous west-dipping reflectors are aligned with each other and project to the surface trace of a NW-dipping Quaternary fault at about s.p.164 in line 111 (Fig. 10).

The main production area. Seismic lines that image the main geothermal production area of the Coso field reveal two basic types of structures exemplified by a southeast-dipping feature that we refer to as the f_4 reflector, and northwest-dipping features that terminate against it. The f_4 reflector is imaged on line 109 as a distinct southeast-dipping reflector in the depth range of 1828 m to 2134 m beneath s.p. 115 (Fig. 6), and can be traced downdip beneath the main production area of the geothermal field. The f_4 reflector is readily visible on a stacked, unmigrated version of line 109 (Fig. 12), and thus is not an artifact of the Kirchhoff pre-stack depth migration processing.

The f_4 reflector can be projected up-dip to the ground surface approximately 2 km NNW of Sugarloaf Mountain (Fig. 4) in the vicinity of a subdued, ~10 m high scarp separating Mesozoic plutonic rock on the northwest side from pyroclastic valley fill on the southeast side. There is, however, no unequivocal surface evidence of an active fault scarp in this location similar to those observed along the Coso Wash fault. The surface projection location of f_4 also marks the northwestern extent of the rhyolite dome field. Based on its appearance in crossing lines 109 and 110, we estimate that f_4 strikes ~N60°E, dips ~50° to the southeast near the surface, and appears to become listric in nature with depth based on northwest-dipping reflective features that terminate against it.

The moderately to steeply northwest-dipping reflectors above f_4 are visible on line 109 in the 1.0–1.5 km depth range between s.p.153 and 185 (Fig. 6). We have designated these f_5, f_{5a}, and f_{5b}. They appear to terminate abruptly against f_4, and are interpreted to be faults that are antithetic to f_4 (Fig. 6). These reflectors appear to correlate with less well defined reflectors on line 110 between 1.0 and 1.5 km depth between s.p. 163 and 173. On this line they have an apparent north dip, but when correlated with the line 109 reflectors show that they represent faults that strike northeast and dip northwest. The updip projection of these reflectors on line 109 is in the vicinity of a series of northeast-striking faults in the bedrock that were mapped by Whitmarsh (1997).

The "A" reflecting horizon: Brittle-ductile transition. The "A" reflector is a discontinuous, poorly imaged, low-relief feature at a depth of 4.0 to 4.5 km that appears to correlate positively with the base of seismicity beneath the geothermal field (Monastero et al., 2005). The most significant feature of the "A" horizon is that a number of the reflectors on the seismic data set appear to terminate against it or sole into it. The clearest example of this is seen in the relationships between f_4 and "A" on line 109 (Fig. 6). Other examples can be seen in Figures 7 and 10.

Monastero et al. (2005) evaluated the base of seismicity in the Coso region and showed that it was as shallow as ~4.0–4.5 km directly beneath the geothermal field, dropping off to 11 to 12 km outside of the field. Earthquake hypocenters plotted on reflection lines indicate that the "A" horizon is located at or near the base of seismicity (Figs. 10, 11, and 13). Temperature gradients in the geothermal field determined from down-hole measurements range between 85°C and 120°C/km (Monastero and Unruh, 2002), which implies that the temperature in the depth range of the "A" reflector is between 340°C and 480°C. This is within the range at which quartz-rich rocks begin to deform by ductile flow in laboratory experiments (see, for instance, Brace and Kohlstedt, 1980) at strain rates of about 10^{-14}sec^{-1} or lower, which characterize the average geodetic deformation rates in the Coso Range (Monastero et al., 2005). Use of the seismic–aseismic boundary as a surrogate for the brittle-ductile transition in the crust has been shown to be a valid assumption in several other studies crustal structure (Lister and Davis, 1989; Gilpin and Lee, 1978; Maja and McEvilly, 1979; Sibson, 1982; Meissner and Strehlau, 1982; Chen and Molnar, 1983, and Smith and Bruhn, 1984).

Given the fact that the "A" horizon is at, or near, the base of observed seismicity, and down-hole temperatures are high enough to permit ductile flow of

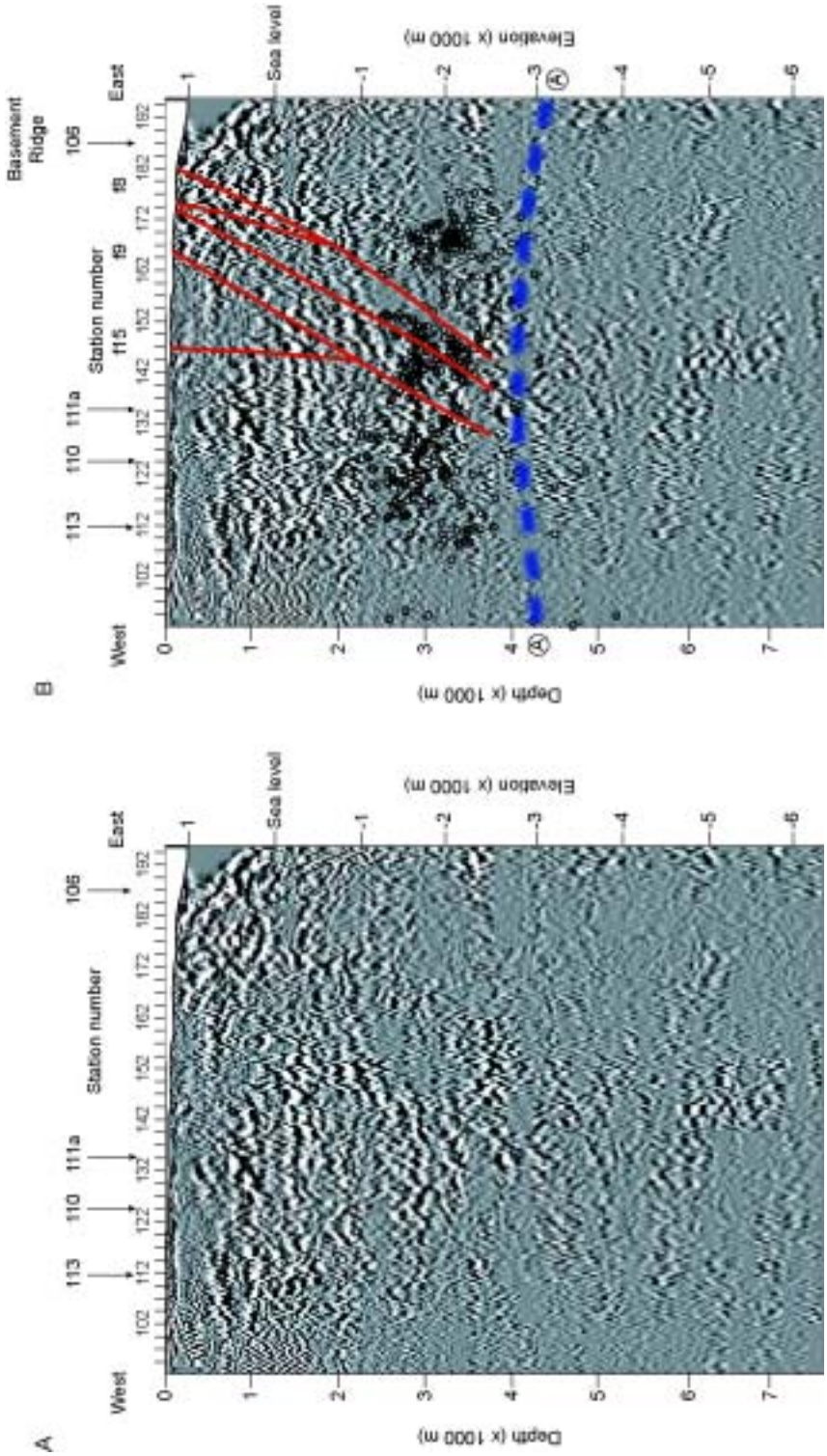

FIG. 10. Reflection line 111. A. Seismic data. B. Interpretation. Hypocenters of local microearthquakes (black dots) projected onto the plane of the seismic section.

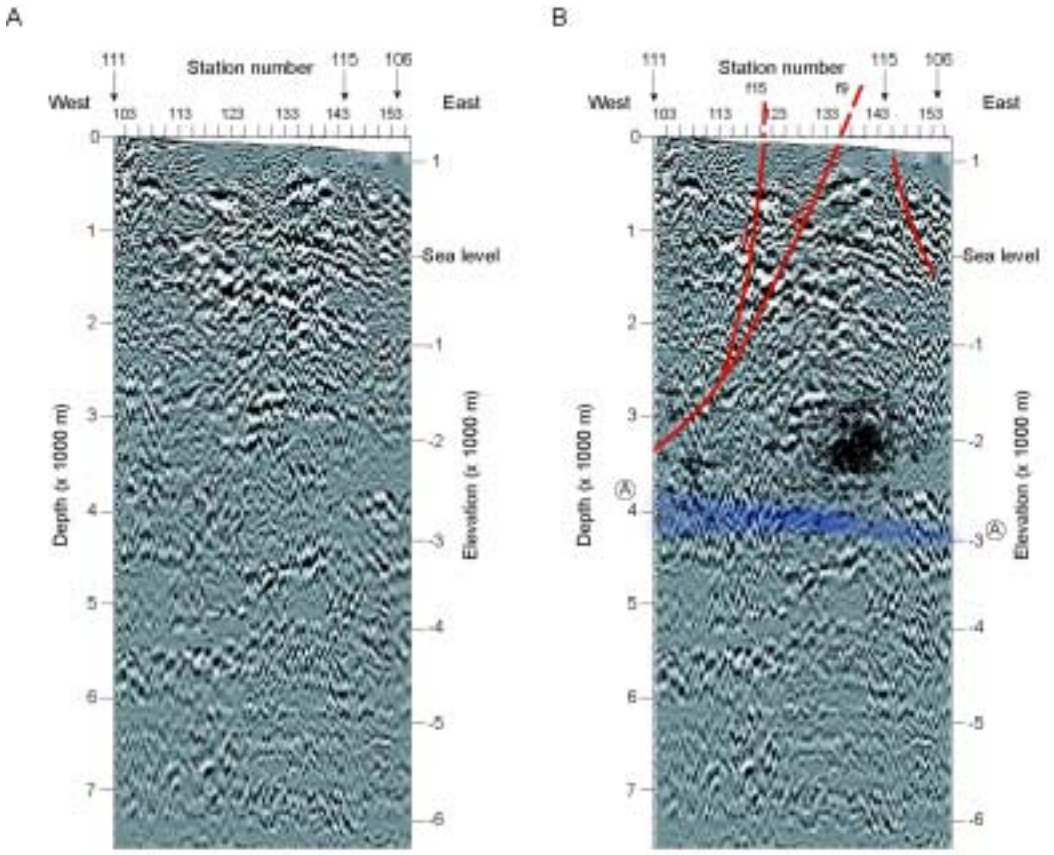

FIG. 11. Reflection line 111a. A. Seismic data. B. Interpretation. Hypocenters of local microearthquakes (black dots) projected onto the plane of the seismic section.

felsic, quartz-rich rocks, we interpret the "A" horizon as a reflective zone on line 109 associated with impedance contrasts along the brittle-ductile transition zone. The fact that some of the faults we interpret from the seismic data also appear to go listric as they approach the "A" horizon (e.g., f_4 on Fig. 6) is also consistent with the analysis of Monastero et al. (2005), wherein they determined from kinematic data derived from microearthquake focal mechanisms that the faults became listric as they approached the brittle-ductile transition. The "A" horizon does not appear as well defined on any of the other seismic lines which may be due to anisotropy of the acoustic velocity field resulting from ductile strain. We thus have not shown the "A" horizon on the other seismic lines, but note that fault reflectors in the data do not extend to depths greater than 4–4.5 km anywhere in the data set.

"C" and "D" reflectors. Two additional reflectors that appear on line 109 (Figs. 12 and 13), horizons "C" and "D," are worthy of mention. Both are high-amplitude features having limited areal extent, and they do not appear on any other seismic lines in this survey. This may be due to the fact that line 109 is longer than any of the others and may permit focusing to greater depths, but in a narrow aperture (i.e., the Fresnel Zone effect), or it may be due to the nature of the reflectors themselves.

The top of horizon "C" occurs at a depth of ~6 km beneath the surface, is subhorizontal in the plane of the seismic section, has a lateral extent of 3 km, and a vertical extent of ~1 km. The dimensions of the "D" horizon reflector is approximately the same as those of the "C" reflector, except that the top lies at a depth of ~8 km to 9 km (Fig. 13). Based on the observations of the base of seismicity

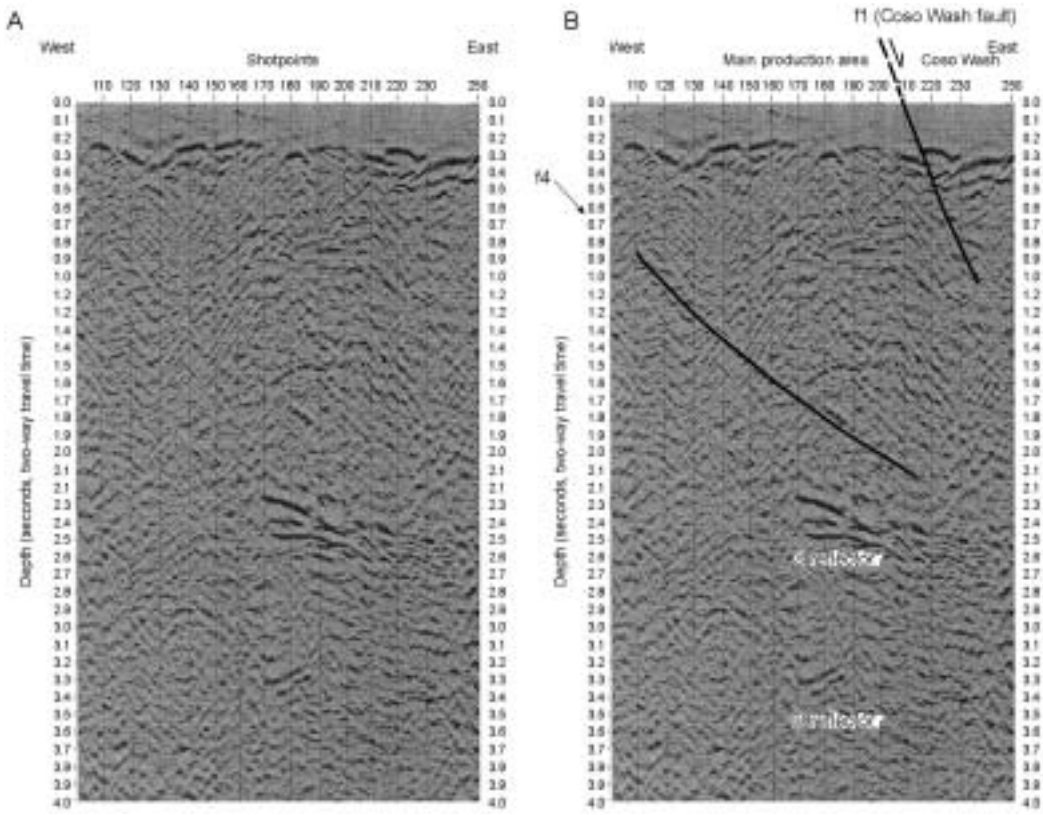

FIG. 12. Stacked version of reflection line 109. A. Seismic data. B. Interpretation.

described in the previous section, both of these reflectors are beneath the brittle-ductile transition in the Coso geothermal field.

The "C" and "D" reflectors can be associated with zones of low acoustic velocities identified by earlier seismological studies of crustal structure in the Coso region. Reasenberg et al. (1980) analyzed teleseismic P-wave arrivals and found that there is a distinct low-velocity body somewhere in the depth range of 5 and 20 km. Those authors attributed the shallowest part of this feature to the presence of a partial melt in the middle crust, which they correlated with local seismic, geologic, and heat flow data. Based on receiver function analysis of converted phases from teleseismic P- and S-waves, Wilson et al. (2003) identified a 2 km thick, upper crustal negative (UCN) velocity zone beneath Coso. The top of the UCN occurs at approximately 4 km depth which correlates closely with the "C" horizon. These latter authors postulated that this feature was the top of a partial (a few percent) melt zone. Wilson et al. (2003) did not reference a well-defined velocity anomaly at 8 km to 9 km depth, although their data indicate a positive velocity anomaly in that depth range that could possibly be the base of the melt zone.

Hauksson and Unruh (2007) evaluated the 3-D velocity structure beneath the Coso Range through joint hypocentral inversion of earthquakes. They imaged a well-defined, NW-SE–trending, low P-wave velocity anomaly beneath the central Coso Range, the top of which is located at a depth of about 5 km beneath the geothermal field and is associated with the lower limit of seismicity. This low Vp anomaly also is associated with anomalous low shear-wave velocities. Based on the low P- and S-wave velocities derived from the inversion, as well as the observation that Vp/Vs and Poisson's ratio do not vary significantly above 10 km depth, Hauksson and Unruh (2007) interpreted the low Vp anomaly in the

5 km to 10 km depth range to be associated with rocks containing about 4–6% geothermal brines. Hauksson and Unruh (2007) observed another low Vp and low Vs anomaly at about 10 km depth characterized by moderately elevated Vp/Vs and Poisson's ratio, and suggested that this deeper velocity anomaly may represent a 2% to 5% volume fraction of magma. From comparison with the results of Hauksson and Unruh (2007), the "C" horizon is spatially associated with the low velocity zone interpreted to contain geothermal brines, and the "D" horizon is associated with the zone of elevated Vp/Vs that may contain magma.

Additional evidence for a magmatic origin of the C and D reflectors is the interpretation by Manley and Bacon (2000) that magmas erupted in the Pleistocene Coso volcanic field were derived from sources at two distinct depths. Based on rhyolite thermobarometry and radiometric age dating, volcanic domes emplaced in the Coso field between 0.6 Ma and 0.3 Ma were derived from a magma source located at a depth of about 10 km. Domes emplaced around 40 ka, however, were derived from a source at 5.5 km depth. Manley and Bacon (2000) suggested that these relations indicate shallowing of the magmatic reservoir between 0.3 Ma and 40 ka. It is possible that remnants of the deeper reservoir that sourced the 0.6–0.3 Ma eruptions are represented by the "D" reflector at ~ 8 km to 9 km depth, and the 40 ka reservoir is imaged as the "C" reflector at about 6 km depth. As noted by Hauksson and Unruh (2007), the values of Vp/Vs and Poisson's ratio beneath the Coso Range suggest that brines rather magma are present in the vicinity of the "C" reflector. If this is correct, then the shallow 40 ka magma reservoir inferred by Manley and Bacon (2000) may have been depleted during the late Pleistocene eruptive sequence.

Discussion

Identification of the major reflectors in the brittle upper crust of the Coso field provides a framework for comparison with upper crustal structures of known metamorphic core complexes. Based on our analysis of the seismic reflection data, we recognize four types of prominent reflectors in the Coso data: (1) the ESE- and NNW-dipping normal faults bounding the prominent north-south–trending basement ridge on the western boundary of Coso Wash; (2) the northeast-striking, southeast-dipping f_4 reflector and the antithetic faults beneath, and west of, the geothermal field; (3) the low-relief, reflective "A" horizon; and (4) the "C" and "D" reflectors at 6 km and 9 km depth, respectively, within low velocity zones beneath the central Coso Range.

The relative locations and geometry of these features are shown in a schematic diagram of the structure of the central Coso Range (Fig. 14). The brittle faults appear to sole into, or terminate against, the "A" horizon at about 4–5 km depth, which we associate with the brittle-ductile transition zone. Most seismicity in the vicinity of the geothermal field and western Coso Wash graben is confined to the upper 4 km above the "A" reflector (e.g., Fig. 13). The high-amplitude "C" and "D" reflectors beneath the brittle-ductile transition may be magma bodies or pockets of lithostatically pressured, superheated magmatic brine derived from a deeper magma source (Fournier, 1999; Hauksson and Unruh, 2007). The magma or fluids provide a localized source of heat that confines brittle deformation to the upper 4.0 to 4.5 km and drives hydrothermal circulation in the field.

A comparison of the Coso structure (Fig. 13) with the general model for a metamorphic core complex in Figure 1 reveals several key similarities, the most important of which is a series of normal faults that accommodate brittle extension above a shallow brittle-ductile transition zone. The key difference between Coso and the general core complex model is in the geometry of the upper plate. In many exhumed core complexes, the upper plate has been arched into an antiform (Fig. 1), presumably a consequence of localized unroofing of the lower plate in the center of the structure with progressive extension. With sufficient cumulative deformation and exhumation, the end result of this process is surface exposure of the brittle-ductile transition zone and underlying crust that has been deformed by ductile flow. Because Coso is a "nascent" core complex that has experienced a few kilometers of horizontal extension or less (Monastero et al., 2005), the unroofing process is in an early stage and has not yet produced significant antiformal relief on the upper plate.

The structural cartoon in Figure 14 prompts other comparisons between Coso and well-studied core complexes. For example, potential analogs to the ESE- and NNW-dipping normal faults at Coso are described by Ingersoll et al. (1996) in their investigation of the Mud Hills area of the Waterman Hills metamorphic core complex in the central Mojave Desert. These authors show a complex

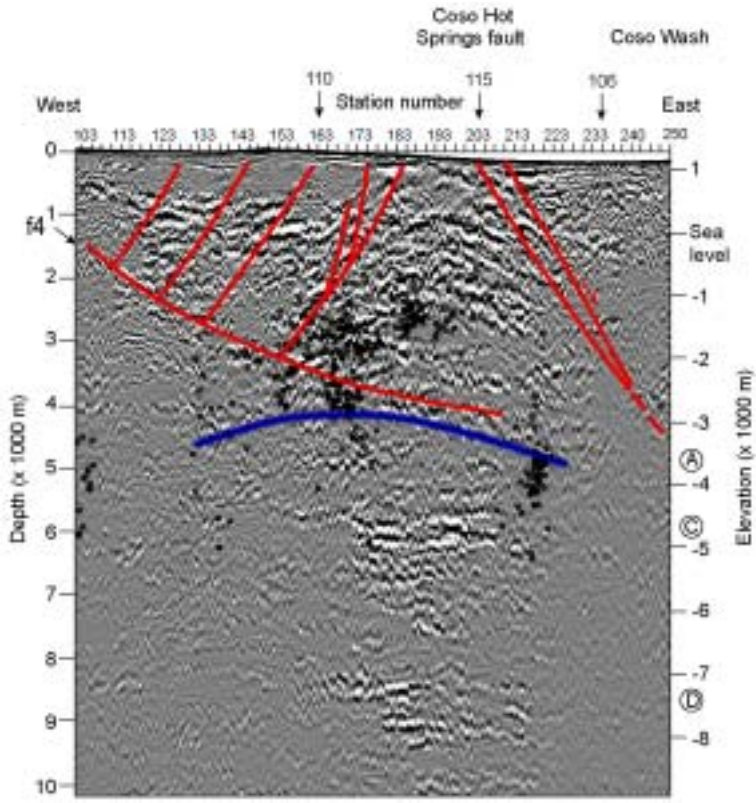

FIG. 13. Pre-stack migration of line 109 to image "D" reflector in 8–9 km depth range. Interpretation of shallow structures as in Figure 9. Hypocenters of local microearthquakes projected onto the plane of the seismic section.

pattern of anastamosing synthetic and antithetic normal faults, in an area approximately 0.5 to 1.0 km wide and 5 km long, that formed perpendicular to the extension direction and parallel to the breakaway fault. This pattern resulted from a succession of normal faults that, once formed, were cut by later faults promulgated by stretching of the upper plate in, or near, the breakaway zone. Many of these normal faults show listric character in the downdip direction (Ingersoll et al., 1996). In the case of the Coso field, this fault pattern reaches from 0.5 to 2.5 km in width and is found in the prominent 23 km long fault-bounded basement ridge bordering western Coso Wash. In their analog modeling investigations of brittle structures in the Coso transtensional setting, Dooley et al. (2004) showed that development of such a ridge is characteristic of the area associated with the breakaway fault and is underlain by the shallowest part of the brittle-ductile transition. The shallow nature of the brittle-ductile transition in the field is confirmed by the very high temperatures (~350°C) in geothermal production wells within the central ridge, and the shallow seismic-aseismic boundary in this area (Monastero and Unruh, 2002; Monastero et al., 2005).

Reflector f_4 may be a fault related to the initial phase of extension in the Coso geothermal field. Monastero et al. (2005) documented systematic variations in the style of seismogenic faulting with depth beneath the geothermal field that suggest earthquakes below about 3 km depth are occurring by simple shear on subhorizontal and/or subvertical faults. The listric nature of f_4 is consistent with one of these low-angle structures. If future extension in the central Coso Range remains localized in the vicinity of the basement ridge (Fig. 14), the ductile crust may rise and produce antiformal relief on the brittle-ductile transition beneath the basement

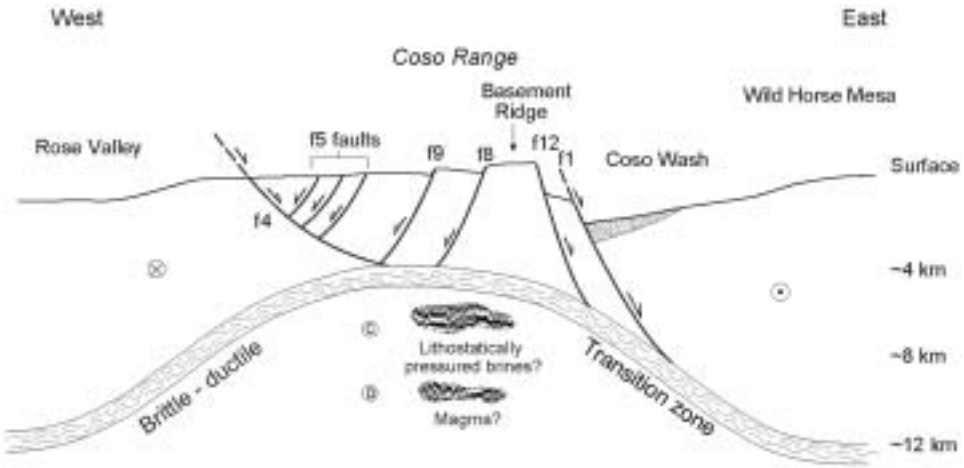

FIG. 14. Structural cartoon of the Coso geothermal field at the latitude of the geothermal field illustrating faults and magmatic features interpreted from reflection seismic, earthquake, and field data. Horizontal extension within the plane of the cross section is driven by a right-releasing transfer of NW-dextral shear across the central Coso Range. Compare with Figure 1.

ridge. If this occurs, then reflector f_4 predictably would be tilted back toward the west, resulting in a geometry similar to that in the general core complex model (Fig. 1). By comparison, the f_4 reflector and associated antithetic faults that occur in the western part of the Coso geothermal field are analogous to a supracrustal basin (cf. the Schell Creek fault and adjacent Spring Valley in Gans et al., 1985). The unnamed fault at Coso is the brittle portion of the detachment fault that separates the upper plate from the lower plate. Gans et al. (1985) acknowledged that the distal (relative to the breakaway fault) 10 km of the northern Snake Range detachment fault behaved as a brittle fault despite the fact that it is rooted in the brittle-ductile transition (see Fig. 1). The brittle-ductile transition beneath Coso deepens quickly in a westerly direction, and we can see that the f_4 fault soles into the "A" horizon at a depth of 1220 m beneath the central part of the geothermal field.

The majority of the seismicity in the upper 3 km beneath the geothermal field probably is related to production and injection of geothermal fluids, and thus is a good indication of where permeable zones are. Well-defined clusters of hypocenters on seismic lines 109 and 111 (Figs. 13 and 10, respectively) are associated with downdip continuations of the NW-dipping Quaternary faults. We interpret that these structures provide permeable pathways for upwelling geothermal fluids heated by magma or lithostatically pressured brines ("C" reflector) below the brittle-ductile transition zone (Fig. 14). These relations recall a generalized model by Fournier (1999) for hydrothermal processes in magmatic-epithermal environments. In Fournier's model, emplacement of a magma body may locally elevate the brittle-ductile transition zone to shallow depths. The transition zone separates a hydrostatically pressured domain above, in which meteoric water flows convectively, from a domain below that deforms by ductile flow.

Because Quaternary magmatism and volcanism in the Coso Range have occurred in a regional transtensional regime, it is reasonable to assume that the intrusive rocks and intrusive bodies at depth may be involved in the crustal-scale deformation. As shown on Figure 14, there is net dextral motion in and out of the plane of maximum WNW-directed extension across the central Coso Range (Unruh et al., 2002). We assume that ductile deformation beneath the central Coso Range includes a component of northwest dextral shear in addition to WNW-ESE extension. Exhumed synkinematic plutons in the Sierra Nevada (Titus et al., 2005) and Canadian Appalachians (Pe-Piper et al., 1998), interpreted to have intruded in local extensional stepovers, pull-apart basins, and/or tension fractures along coeval dextral shear zones, may provide insights into

ductile processes occurring at depth beneath the Coso Range:

1. Analysis of penetrative structural and magnetic fabrics in the Cretacous Johnson Granite and Silver Pass Porphyries in the central Sierra Nevada indicate synkinematic flow in both the magmatic and high-temperature solid states (Titus et al., 2005). The foliations generally are steeply dipping to subvertical, and lineations plunge shallowly, indicating distributed shearing deformation consistent with emplacement in a strike-slip tectonic regime.

2. The Late Devonian Pleasant Hills pluton in the Canadian Appalachians was interpreted by Pe-Piper et al. (1998) to have been emplaced along a positive flower structure associated with the dextral Coequid fault zone. The pluton was assembled in several distinct episodes that included intrusion of vertical sheets and larger, massive bodies along splays of Coequid fault zone. Based on the orientations of individual intrusive sheets relative to the strike of the fault zone, Pe-Piper et al. (1998) interpreted that magma variously intruded along the component faults of the Coequid zone, including P, R, and R' shears, and normal and reverse faults. Structural fabrics are preserved that record penetrative deformation of the plutons in both magmatic and solid states.

If the analogy with these ancient, exhumed plutons is correct, then deformation below the brittle-ductile transition at Coso may be localized along ductile shear zones of finite width that are preferred zones for magmatic intrusion. Alternatively, ductile shear at depth may preferentially be localized within young, hot dikes whose orientations are controlled by the regional strain geometry. Titus et al. (2005) suggest that the Johnson Granite Porphyry intruded along a 3-D tension gash at the tip of a strike-slip fault and possibly fed a rhyolite dome field at the surface. In the case of the central Coso Range, the late Pleistocene rhyolite field and underlying magmatic features occur within an extensional stepover rather than a large-scale tension gash. Although the kinematics of deformation are somewhat different in the two examples, the common element is that extension and magmatism are localized by geometric complexities in a strike-slip system. We suggest that a composite cross-section of the upper 15 km of crust in a transtensional/magmatic orogen may be constructed using the following areas as analogs: the central Coso Range as an example of brittle surface faulting, volcanism, and hydrothermal convection in the upper 4 to 5 km (this paper); the Black Mountains metamorphic core complex in Death Valley as an example of the structures directly above and below the brittle-ductile transition in the depth range of 4 to 8 km (Holm and Wernicke, 1990; Serpa and Pavlis, 1996); and the Cretaceous synkinematic plutons in the Sierra Nevada for magmatic processes and ductile deformation between about 8 and 15 km (Titus et al., 2005).

Conclusions

The processing approach used for this study demonstrates that reflection seismology can be successfully employed to image the subsurface structure of a geothermal field hosted in crystalline (i.e., acoustically "transparent") rocks. Depth-migrated images that incorporate detailed velocity data reveal substantial reflective structure in the upper crust, including brittle faults and deeper features that are possibly related to magmatic activity. Based on analysis of the reflection images, we conclude that tectonic extension of the upper 4 km of the crust is accommodated by brittle faulting within the Coso field and opening of the Coso Wash graben to the east. The brittle faults appear to sole into or terminate against a sub-horizontal reflecting "A" horizon at about 4 km depth that we associate with the transition from brittle faulting to ductile flow. Ductile stretching of the crust and emplacement of shallow igneous bodies and/or magmatic brines (the "C" and "D" reflectors) may accommodate extension at depth, particularly beneath the geothermal field. The intrusions provide a localized source of heat that confines brittle deformation to the upper 4 km of the crust and drives hydrothermal circulation in the field. The relationship between the upper crustal faults, brittle-ductile transition zone, and deep magmatic features is consistent with the interpretation of Monastero et al. (2005) that the Coso geothermal field is a nascent metamorphic core complex related to oblique transtensional deformation along the southeastern margin of the Sierra Nevada microplate.

Acknowledgments

This work was supported by the U.S. Navy Geothermal Program Office. The authors are grateful to J. D. Walker and E. M. Moores for their constructive reviews, which prompted improvements to the final paper.

REFERENCES

Argus, D. F., and Gordon, R. G., 1991, Current Sierra Nevada–North America motion from very long baseline interferometry: Implications for the kinematics of the western United States: Geology, v. 19, p.1085–1088.

Argus, D. F., and Gordon, R. G., 2001, Present tectonic motion across the Coast Ranges and San Andreas fault system in central California: Geological Society of America Bulletin, v. 113, p. 1580–1592.

Asad, A. M., Pullammanappallil, S. K., Anooshehpoor, A., and Louie, J. N., 1999, Inversion of travel time data for earthquake locations and three-dimensional velocity structure in the Eureka Valley area, eastern California: Bulletin of the Seismological Society of America, v. 89, p. 796–810.

Brace, W. F., and Kohlstedt, D. L., 1980, Limits on lithospheric stress imposed by laboratory experiments: Journal of Geophysical Research, v. 859, p. 6248–6252.

Buck, W. R., 1988, Flexural rotation of normal faults: Tectonics, v. 7, p. 959–973.

Chen, P., and Molnar, P., 1983, The depth distribution of intracontinental and intraplate earthquakes and its implications for the thermal and mechanical properties of the lithosphere: Journal of Geophysical Research, v. 88, p. 4183–4214.

Christensen, N. I., 1996, Poisson's ration and crustal seismology: Journal of Geophysical Research, v. 101, p. 3139–3156.

Coney, P. J., 1979, Tertiary evolution of Cordilleran metamorphic core complexes, *in* Armentrout, J. W., Cole, M. R., and Terbest, H., eds., Cenozoic paleogeography of the Western United States: Society of Economic Paleontologists and Mineralogists, Pacific Section Symposium 111.

Dewey, J. F., Taylor, T. R., and Monastero, F. C., 2008, Transtension in the Brittle Field: The Coso Region, Southern California: International Geology Review, v. 50, no. 3, **pp. xx-xx[AB: add final page numbers when known].**

Dixon, T. H., Miller, M., Farina, F., Wang, H., and Johnson, D., 2000, Present-day motion of the Sierra Nevada block and some tectonic implications for the Basin and Range province, North American Cordillera: Tectonics, v. 19, p. 1–24.

Dixon, T. H., Robaudo, J. L., and Reheis, M. C., 1995, Constraints on present-day Basin and Range deformation from space geodesy: Tectonics, v. 14, p. 755–772.

Dokka, R. K., and Travis, C. J., 1990, Late Cenozoic strike-slip faulting in the Mojave desert: Tectonics, v. 9, p. 311–430.

Dooley, T., Monastero, F. C., Hall, B., McClay, K., and Whitehouse, P., 2004, Scaled sandbox modeling of transtensional pull-apart basins—applications to the Coso geothermal system: Geothermal Resources Council, Transactions, v. 28, p. 637–641.

Duffield, W. A., and Bacon, C. R., 1981, Geologic map of the Coso volcanic field and adjacent areas, Inyo County, California: U.S. Geological Survey Miscellaneous Investigations Series Map I-1200, scale 1:50,000.

Duffield, W. A., Bacon, C. R., and Dalrymple, G. B., 1980, Late Cenozoic volcanism, geochronology, and structure of the Coso Range, Inyo County, California: Journal of Geophysical Research, v. 85, p. 2381–2404.

Eaton, D. W., Milkereit, B., and Salisbury, M., 2003, Seismic methods from deep mineral exploration: Mature technologies adapted to new targets: The Leading Edge, v. 22, p. 580–585.

Fillmore, R. P., and Walker, J.D., 1996, Evolution of a supradetachment extensional basin: The lower Miocene Pickhandle Basin, central Mojave Desert, California, *in* Beratan, K. K., ed., Reconstructing the history of Basin and Range extension using sedimentology and stratigraphy: Boulder, CO, Geological Society of America Special Paper 303, p. 107–126.

Fillmore, R. P., Walker, J. D., Bartley, J. M., and Glazner, A. F., 1994, Development of three genetically related basins associated with detachment-style faulting: Predicted characteristics and an example from the central Mojave Desert, California: Geology, v. 22, p. 1087–1090.

Fournier, R., 1999, Hydrothermal processes related to movement of fluid from plastic into brittle rock in the magmatic-epithermal environment: Economic Geology, v. 94, p. 1193–1212.

Gans, P. B., Miller, E. L., McCarthy, J., and Ouldcutt, M. L., 1985, Tertiary extensional faulting and evolving brittle-ductile transition zones in the northern Snake Range and vicinity: New insights from seismic data: Geology, v. 13, p. 189–193.

Gilpin, B., and Lee, T. C., 1978, A microearthquake study of the Salton Sea geothermal area, California: Seismological Society of America Bulletin, v. 68, p. 441–450.

Hauksson, E., and Unruh, J., 2007, Regional tectonics of the Coso geothermal area along the intra-continental plate boundary in central-eastern California: Three-dimensional V_P and V_P/V_S models, spatial-temporal seismicity patterns, and seismogenic strain deformation: Journal of Geophysical Research, v. 112 [doi:10.1029/2006JB0044721].

Holm, D., and Wernicke, B., 1990, Black Mountains crustal section, Death Valley extended terrain, California: Geology, v. 18, p. 520–523.

Ingersoll, R. V., Devaney, K. A., Geslin, J. K., Cavazza, W., Diamond, D. S., Heins, W. A., Jagiello, K. J., Marsaglia, K. M., Paylor, E. D., II, and Short, P. F., 1996, The Mud Hills, Mojave Desert, California: Structure, stratigraphy, and sedimentology of a rapidly extended terrane, *in* Beratan, K. K., ed., Reconstructing the history of Basin and Range extension using sedimen-

tology and stratigraphy: Boulder, CO, Geological Society of America Special Paper 303, p. 61–84.

Jennings, C. W., 1994, Fault activity map of California and adjacent areas: California Department of Conservation, Division of Mines and Geology, Geologic Data Map No.6, scale 1:750,000.

Juhlin, C., and Palm, H., 1999, 3-D structure below Ävrö Island from high-resolution reflection seismic studies, southeastern Sweden: Geophysics, v. 64, p. 662–667.

Julian, B. R., Foulger, G. R., and Monastero, F. C., 2007, Microearthquake moment tensors from the Coso geothermal area, *in* Proceedings, 32nd Workshop on Geothermal Reservoir Engineering, Stanford University, Stanford, CA, January 22–24, 2007, p. 373–377.

Kim, J. S., Moon, W. M., Lohga, G., Serzu, M., and Soonawala, N., 1994, Imaging of reflection seismic energy for mapping shallow fracture zones in crystalline rocks: Geophysics, v. 59, p. 753–765.

Lister, G. S., and Davis, G. A., 1989, The origin of metamorphic core complexes and detachment faults formed during Tertiary continental extension in the northern Colorado River region, U.S.A.: Journal of Structural Geology, v. 11, nos. 1/2, p. 65–94.

Mair, J. A., and Green, A. G., 1981, High-resolution seismic reflection profiles reveal fracture zones within a "homogeneous" granite batholith: Nature, v. 294, p. 439–442.

Maja, E. L., and McEvilly, T., 1979, Seismological investigations at the Geysers geothermal field: Geophysics, v. 44, p. 246–269.

Manley, C. R., and Bacon, C. R., 2000, Rhyolite thermobarometry and the shallowing of the magma reservoir, Coso volcanic field, California: Journal of Petrology, v. 41, p. 149–174.

Meissner, R., and Strehlau, J., 1982, Limits of stresses in continental crusts and their relation to the depth-frequency distribution of shallow earthquakes: Tectonics, v. 1, p. 73–89.

Monastero, F. C., Katzenstein, A. M., Miller, J. S., Unruh, J. R., Adams, M. C., and Richards-Dinger, K., 2005, The Coso geothermal field: A nascent metamorphic core complex: Geological Society of America Bulletin, v. 117, p.1534–1553.

Monastero, F. C., and Unruh, J. R., 2002, Definition of the brittle-plastic transition in the Coso geothermal field, east-central California, USA: EAGE 64th Conference and Exhibition, Florence, Italy, May 27–30.

Monastero, F. C., Walker, J. D., Katzenstein, A. M., and Sabin, A. E., 2002, Neogene evolution of the Indian Wells Valley, east-central California, *in* Glazner, A. F. et al., eds., Geologic evolution of the Mojave Desert and southwestern Basin and Range: Boulder, CO, Geological Society of America Memoir 195, p. 199–228.

Optim LLC, 2003, Detailed three-dimensional acoustic velocity analysis of the Coso geothermal field: Report prepared for the U.S. Navy Geothermal Program Office, China Lake, California, Contract #N68936-02-P-0442.

Pe-Piper, G., Koukouvelas, I., and Piper, D. J. W., 1998, Synkinematic granite emplacement in a shear zone: The Pleasant Hills pluton, Canadian Appalachians: Geological Society of America Bulletin, v. 110, p. 523–536.

Pullammanappallil, S. K., Honjas, W., Unruh, J. R., and Monastero, F. C., 2001, Use of advanced data processing techniques in the imaging of the Coso geothermal field, *in* Proceedings, 26th Workshop on Geothermal Reservoir Engineering, Stanford, California.

Pullammanappallil, S. K., and Louie, J. N., 1993, Inversion of seismic reflection traveltimes using a nonlinear optimization scheme: Geophysics, v. 58, p. 1607–1620.

Pullammanappallil, S. K., and Louie, J. N., 1994, A generalized simulated-annealing optimization for inversion of first-arrival times: Bulletin of the Seismological Society of America, v. 84, p. 1397–1409.

Reasenberg, P., Ellsworth, W., and Walter, A., 1980, Teleseismic evidence for a low-velocity body under the Coso geothermal resource area: Journal of Geophysical Research, v. 85, p. 2471–2483.

Roquemore, G. R., 1981, Active faults and associated tectonic stress in the Coso Range, California: Naval Weapons Center Technical Publication 6270, 101 p.

Roquemore, G. R., and Zellmer, J. T., 1983, Airport Lake and Little Lake faults: Ground cracking associated with the 1982 magnitude 5.2 Indian Wells Valley earthquake: California Geology, v. 36, p. 197–200.

Salisbury, M. H., Harvey, C. W., and Matthews, L., 2003, The acoustic properties of host rocks in hardrock terranes, *in* Eaton, D. W. et al., eds., Hardrock exploration: Society of Exploration Geophysicists, Geophysical Development No. 10, p. 9–19.

Salisbury, M. H., Milkereit, B., and Bleeker, W., 1996, Seismic imaging of massive sulfide deposite, Part 1. Rock properties: Economic Geology, v. 91, p. 821–828.

Serpa, L. and Pavlis, T. L., 1996, Three-dimensional model of the late Cenozoic history of the Death Valley region, southeastern California: Tectonics, v. 15, p. 1113–1128.

Sibson, R. H., 1982, Fault zone models, heat flow, and depth distribution of seismicity in the continental crust of the United States: Seismological Society of America Bulletin, v. 72, p. 151–163.

Smith, R. B., and Bruhn, R. L., 1984, Intraplate extensional tectonics of the eastern Basin-Range: Inferences on structural style from seismic reflection data, regional tectonics, and thermal-mechanical models of brittle-ductile deformation: Journal of Geophysical Research, v. 89, p. 5733–5762.

Spencer, J. E., 1984, The role of tectonic denudation in the warping and uplift of low-angle normal faults: Geology, v. 12, p. 95–98.

Titus, S. J., Clark, R., and Tikoff, B., 2005, Geological and geophysical investigation of two fine-grained granites, Sierra Nevada Batholith, California: Evidence for structural controls on emplacement and volcanism: Geological Society of America Bulletin, v. 117, p. 1256–1271.

Unruh, J. R., Hauksson, E., Monastero, F. C., Twiss, R. J., and Lewis, J. C., 2002, Seismotectonics of the Coso Range-Indian Wells Valley region, California: Transtensional deformation along the southeastern margin of the Sierran microplate, *in* Glazner, A. F., Walker, J. D., and Bartley, J. M., eds., Geologic evolution of the Mojave Desert and southwestern Basin and Range: Boulder, CO, Geological Society of America Memoir 195, p. 277–294.

Unruh, J. R., Humphrey, J., and Barron, A., 2003, Transtensional model for the Sierra Nevada frontal fault system, eastern California: Geology, v. 31, p. 327–330.

Vidale, J. E., 1990, Finite-difference calculation of travel times: Bulletin of the Seismological Society of America, v. 78, p. 2062–2076.

Walker, J. D., and Whitmarsh, R. W., 1998, A tectonic model for the Coso geothermal area: U.S. Department of Energy Proceedings, Geothermal Program Review XVI, April 1–2, Berkeley, CA, p. 2–17 to 2–24.

Wernicke, B. P. 1992, Cenozoic extensional tectonics of the U.S. Cordillera, *in* Burchfiel, B. C. et al., eds., The Cordilleran orogen: Conterminous U.S.: Boulder, CO, Geological Society of America, Geology of North America, v. G-3, p. 553–581.

Whitmarsh, R. W., 1997, New and compiled mapping of the central Coso Range: Available in ArcInfo-compatible format from the University of Kansas, Department of Geology, Structural Geology and GIS Laboratory (http://geomaps.geo.ukans,edu/html/coso.html).

Wilson, C. K., Jones, C. H., and Gilbert, H. J., 2003, Single-chamber silicic magma system inferred from shear wave discontinuities of the crust and uppermost mantle, Coso geothermal area, California: Journal of Geophysical Research, v. 108 [doi:10.1029/2003].